Quasi-Classical Trajectory Studies of the Insertion Reactions $S(^1D) + H_2$, HD, and D_2†

Sheng Der Chao and Rex T. Skodje*

Department of Chemistry and Biochemistry, University of Colorado, Boulder, Colorado 80309

Received: September 5, 2000; In Final Form: October 16, 2000

In this work, we present the results of a quasi-classical trajectory (QCT) calculation using a newly developed potential energy surface for the title reactions. The integral cross sections, the product state-resolved differential cross sections, the angle-state-specific energy partitions, and other relevant reaction attributes are computed. The QCT integral cross sections, the differential cross sections, and the gross features of the product distributions are consistent with a simple view of the reaction as mediated by capture dynamics in the entrance channel, followed by the statistical decay of a long-lived complex. We present a comparison to the molecular beam experiments of Lee and Liu, which show agreement in the broad pattern of results but also exhibit significant differences in the more finely resolved quantities.

I. Introduction

In the past decade there has been considerable interest, both experimentally and theoretically, in exploring the detailed dynamics of insertion-type chemical reactions, such as $N(^2D) + H_2$[1−5] and $O(^1D) + CH_4$.[6−10] For an insertion reaction of an atom and a diatomic molecule, one chemical bond is broken while two bonds are formed. Thus, we expect the existence of a deep potential well along the reaction path capable of sustaining a long-lived reactive complex. In contrast, direct abstraction reactions generally do not show a deep well, and trapping, if it occurs at all, is quite transitory. Thus, many of the dynamical insights developed in the extensive studies of abstraction reactions may be inapplicable to insertion reactions. To the extent that a "standard model" exists for insertion reactions, it consists of "capture" dynamics involving the entrance channel centrifugal barrier, followed by the statistical decay of a long-lived complex. Although such a statistical-capture theory is quite useful for analyzing rate constant data, a more dynamically detailed analysis may be necessary to interpret less averaged observables such as state-resolved differential cross sections. In this work, we present a theoretical analysis of the $S(^1D) + H_2$ reaction, which we shall argue is dominated by the insertion mechanism.

In previous work,[11−44] the reaction $O(^1D) + H_2 \rightarrow OH + H$ has served as a prototype system for the insertion mechanism. Molecular beam and bulk experiments[11−23] have yielded detailed scattering information for a variety of initial states, isotopes, and final-state observables. Theoretical interest in this reaction has spurred the development of several high-quality ab initio potential energy surfaces (PESs).[24−29] Dynamics calculations employing quasi-classical trajectory (QCT) simulations,[17,18,21,30−34] trajectory surface hopping (TSH),[35−38] and quantum scattering theory[39−44] have been applied to analyze the reaction dynamics. It is difficult to concisely encapsulate all that has been learned from these studies, but several conclusions are useful to review. First, while the insertion mechanism clearly plays a major role in the dynamics, for higher collision energies the abstraction mechanism also contributes to the reaction. The results of both experiment[13−22] and theory[33−39] seem to buttress this conclusion, although the discrepancies between experiment and theory still remain. Recent theoretical studies[35−38,44] also indicate that multiple surface effects might be important in the reaction dynamics, especially manifested in the more detailed product distributions. In addition to the lowest $^1A'$ surface which correlates directly with the $^1A_1$ ground state of the stable H_2O molecule, the reaction is complicated by an abstraction route proceeding along the $1^1A''$ excited-state surface for collision energies larger than about 2 kcal/mol. Furthermore, the $2^1A'$ state couples to the $1^1A'$ state via conical intersection in the complex region. While the nonadiabatic dynamical effects can be simulated using ab initio surface information, it has been difficult to devise a simple dynamical picture that can account for the observed product distributions. Also, while it is clear from the dynamics simulations that much of the reactive flux proceeds through intermediate H_2O^* complexes, some non-statistical effects are apparent.

The $S(^1D) + H_2$ reaction is obviously a close analogue to $O(^1D) + H_2$, but in certain respects it may provide a desirable prototype for the insertion mechanism. On the basis of the Evans−Polanyi relation, which states that the activation energy of a chemical reaction increases with decreasing exoergicity, it was surmised[45] that the abstraction barrier for $S(^1D) + H_2$ may be substantially higher than that for $O(^1D) + H_2$. We have recently presented ab initio calculations that, in fact, show the abstraction barrier increases to about 8 kcal/mol in this reaction.[53] On the other hand, the exothermicity of the $S(^1D) + H_2$ reaction, $\Delta E \approx 7$ kcal/mol, is significantly less than that for $O(^1D) + H_2$, $\Delta E \approx 43$ kcal/mol. This implies, at least for the dynamics occurring on a single PES, that the complex lifetime should be longer for $S(^1D) + H_2$ and, thus, that statistical theory may be a better starting point for the analysis of the dynamics. Our theoretical analysis is motivated by recent molecular beam experiments of Lee and Liu.[45−48] Lee and Liu have carried out molecular beam experiments on the three isotopes over the collision energies $E_C = 0.6-6$ kcal/mol. The integral cross sections, vibrational-state-resolved differential cross sections, and angle-resolved translational energy distributions were measured. Some aspects of the results were clearly consistent with the simple capture/decay model of the dynamics. However, the more highly resolved angular product distributions, and some

† Part of the special issue "Aron Kuppermann Festschrift".

10.1021/jp003184c CCC: $20.00
Published on Web 12/15/2000

of the isotope effects, were very suggestive of nonstatistical reaction dynamics. It is useful at this point to consider the predictions of theoretical simulations to test to what extent the theoretical dynamics may explain the observations.

Since relatively little is known about the $S(^1D) + H_2$ reaction, in this work we restrict our analysis to a simple QCT treatment of the reaction dynamics restricted to a single potential surface. While the limitations of such a treatment are clear, it provides a starting point for further dynamical analysis. Furthermore, despite approximation, classical mechanics does allow visualization and physical interpretation of the reaction dynamics. We shall present QCT results for most of the available experimental observables and present a discussion of the agreement (and disagreement) between theory and experiment. In section II, we describe the potential energy surface and some details of the QCT simulations. In section III, we present a comprehensive comparison of the QCT results with the experimental results. In section IV, we discuss the physical implications of our findings, and present some ideas to account for differences with experiment.

II. Theoretical Methods

A. Potential Energy Surface. In a recent report,[53] we have presented a global representation of the lowest PES for the $S(^1D) + H_2$ system. The surface was constructed by fitting a large grid of ab initio points to a global potential function. Here, we review some of the previous discussion concerning the construction of the surface.

The reaction of the $S(^1D)$ atom with H_2 leads to five degenerate surfaces in the initial asymptotical region which correlate to the state $S(^1D) + H_2(X\ ^1\Sigma^+)$. These five potential surfaces have Σ, Π, and Δ symmetries in linear geometry. The Σ surface is the lowest in the entrance channel but correlates to the excited A state of the product SH. The Π surface correlates to the ground-state product in linear geometry but splits into A′ and A″ for bent geometry. The Σ surface has A′ symmetry in nonlinear geometry, and it mixes with the A′ component from the Π surface to form the lowest ^{1}A′ surface in C_s symmetry.

Several large-scale ab initio treatments of the H_2S molecule have been reported previously,[49−52] but these calculations have not been done at enough geometries to simulate the full reaction dynamics. Recently, we have calculated the 1A′, 2A′, 3A′, 1A″, and 2A″ singlet potential energies for the $S(^1D) + H_2$ reaction over an extensive range of geometries.[53] The electronic structure calculation is carried out using the MRCI method employing the augmented polarized quadruple (aug-pvqz) basis set proposed by Dunning et al.[54,55] The active space of the orbitals is optimized by distributing the eight valence electrons over seven active orbitals (three, two, and two from A_1, B_1, and B_2, respectively) with CASSCF and MRCI. The normalized Davidson correction[56] is used for estimating the effects from higher order excitations. A total of 2392 points were calculated on a regular $23 \times 26 \times 4$ grid using the entrance channel Jacobi (R, r, θ) coordinates, where R is the distance between S and the center of mass (com) of H_2, r is the bond distance of H_2, and θ is the angle between vectors **R** and **r**. The ranges of these points are [0.0, 10.0] for R, [0.5, 12.0] for r, and [0.0, 90.0] for θ, in bohrs and degrees. The calculated ground-state surface has fairly accurately reproduced the spectroscopic and thermochemical properties of the stable H_2S molecule and its asymptotes. According to the calculation, the first excited-state surface exhibits a collinear barrier of about 8 kcal/mol, which would be high enough to prevent significant reaction probability through this pathway at the collision energies considered here.

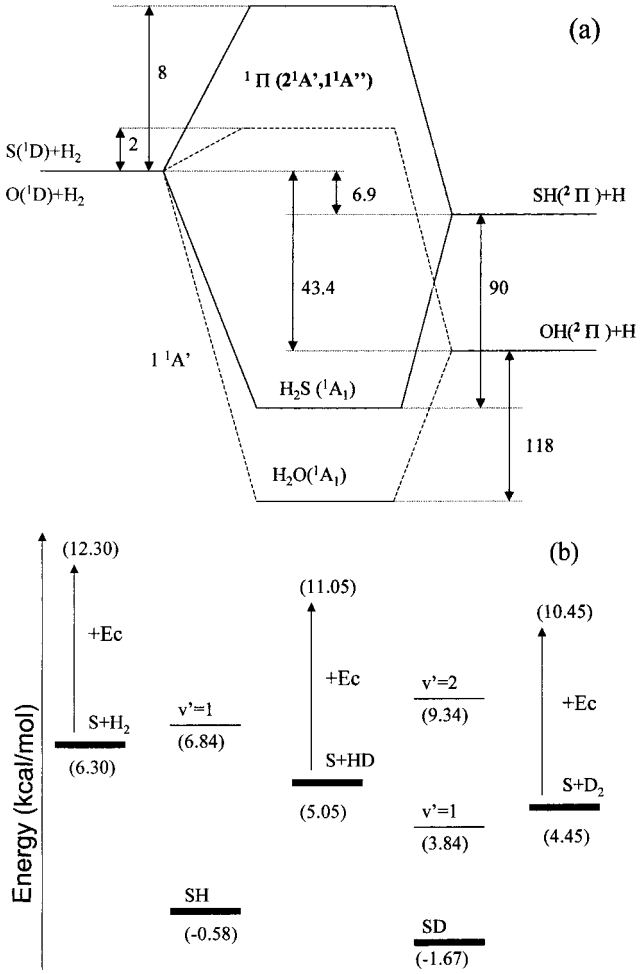

Figure 1. (a) Schematic plot of the energy levels for the $S(^1D) + H_2$ and $O(^1D) + H_2$ reactions. The energy levels are plotted with respect to their corresponding entrance channels. (b) Relevant energetics of the $S(^1D) + H_2/HD/D_2$ reactions. The reagent diatoms are in their lowest internal states ($v = 0$, $j = 0$), with the arrows showing the relevant collision energy ranges for each case. SH and SD are in the lowest internal states ($v' = 0$, $j' = 0$), with the corresponding excited v' states. The numbers in parentheses denote the energy values, with the zero energy referring to the entrance minimum point of the adiabatic PES.

The energetics of the $S(^1D) + H_2$ reaction and the analogous $O(^1D) + H_2$ reaction are schematically depicted in Figure 1a. All the energy levels are referred to the corresponding entrance channels. As can be seen from the plot, both reactions involve deep potential wells (~118 kcal/mol with respect to the OH + H channel for $O(^1D)$ and ~90 kcal/mol with respect to the SH + H channel for $S(^1D)$), but the exoergicity of $S(^1D) + H_2$ reaction is substantially smaller than that of the $O(^1D)$ case (6.9 kcal/mol versus 43.4 kcal/mol). Notice in this plot that the activation barriers to abstraction on the first excited-state surfaces are quite different, ~8 kcal/mol for $S(^1D)$ but 2 kcal/mol for $O(^1D)$. It is therefore anticipated that the abstraction mechanism will show very different energetic thresholds for the two reactions. In Figure 1b we summarize the relevant state energies for the reactions.

The ab initio points were fitted first using the reproducing kernel Hilbert space (RKHS) method used previously to obtain a globally analytical PES for the reaction $O(^1D) + H_2$.[28,57] Briefly, in the RKHS method, the potential energy surface is determined from the Murrell−Sorbie many-body expansion[24,27]

$$V(R_1,R_2,R_3) = V_1 + V_{SH}(R_1) + V_{SH}(R_2) + V_{HH}(R_3) + V_3(R_1,R_2,R_3) \quad (1)$$

where R_1, R_2, and R_3 are the bond distances of S−H, S−H, and H−H, respectively. V_1, V_{SH}, and V_3 are the one-, two-, and three-body potentials. The one-body term is a constant assigned to the value of the three-atom dissociation limit, $S(^3P) + 2H(^2S)$. The two- and three-body potentials are represented by the special functions called "reproducing kernels". The two-body terms are determined by interpolating the ab initio data points for each diatomic species at very large separation. The three-body term is obtained from interpolation of the difference between the calculated ab initio data points and the sum of the one- and two-body terms on the 3D regular grid.

One complicating factor in constructing a single-valued PES for the reaction arises from the two-body potential where the ground state of H_2S has two dissociation channels corresponding to the singlet and the triplet sulfur states, i.e., $S(^1D) + H_2(X\ ^1\Sigma_g^+)$ and $S(^3P) + H_2(a\ ^3\Sigma_u^+)$. The two potential curves intersect at $R_{HH} \approx 3.2\ a_0$ and cause a cusp due to the singlet−triplet splitting. Restricted to low energy scattering from ground-state reactants, this cusp might not significantly affect the results. However, as has been noticed and discussed in studies of the analogous reaction of $O(^1D)$, the cusp complicates the dynamical analysis, especially for the exit channels,[24−27] and also causes problems in fitting the PES. A common way to treat this cusp, which we have adopted, is to compensate for it in the three-body potential, where an anticusp exists, making the full potential smooth and single-valued.

It was found that RKHS fitting produced a smooth and reasonable representation in the entrance channel, and in the well region, but showed unphysical oscillation in the exit channels. This was likely due to the sparseness of ab initio grid points in the product region. To reasonably represent the PES in the exit channels, the Murrell−Carter fitting scheme[26,27] is used. We utilize the available ab initio data points and fit these points to analytical representations of the potentials

$$V(R_\gamma,r_\gamma,\theta_\gamma) = V_{SH}(r_\gamma) + V_3(R_\gamma,r_\gamma,\theta_\gamma) \quad (2)$$

The basis functions and the optimized coefficients are given in ref 53. The PES is constructed in such a way that the long-range behavior for the exit channel $R_\gamma > 4.8\ a_0$ is accurately represented. The Murrel−Carter surface is smoothly joined to the RKHS surface over the interval $R_\gamma = 4.8-5\ a_0$ using the switching function

$$\lambda(x) = x - (\sin(2\pi x)/2\pi) \quad (3)$$

where $x = (R_\gamma - 4.8)/0.2$. The combined potential is then

$$V(R,r,\theta) = V_a + \lambda(x)(V_b - V_a) \quad (4)$$

in which V_a is the RKHS PES and V_b is the Murrel−Carter PES. All the free parameters in the singular value decomposition (SVD) fitting code are optimized so that the local deviations of the two PESs in the connecting region are less than 1.5 kcal/mol.

In Figure 2, the fitted PES in the T-shape geometry is plotted, along with the minimum-energy curve along the R coordinate. The angular anisotropy of the entrance channel potential is displayed in Figure 3, where the PES is plotted holding the H_2 bond length fixed at its equilibrium value.

B. Trajectory Calculation. The QCT calculations are carried out in standard fashion.[58−60] A random distribution of initial conditions is selected for each collision energy for the initial vibrational state $v = 0$ and, separately, initial rotational states $j = 0$, 1, 2, and 3, which is sufficient to simulate the molecular beam rotational temperature. In this way, rotational-state-specific cross sections may be obtained which are combined to obtain the total result. The relative weights are (0.216, 0.744, 0.034, 0.006) for the H_2 case (150 K), (0.490, 0.320, 0.180, 0.010) for the D_2 case (100 K), and (0.82, 0.18, 0.001, 0) for the HD case (50 K). The initial atom−diatom separation is chosen to be $\rho = 20\ a_0$, and the maximum impact parameter for all energy ranges is chosen to be $b_{max} = 12\ a_0$. The trajectories were propagated until $R = 10\ a_0$ with outgoing velocity. For ICS and angle-averaged product distributions, 10000−20000 trajectories per energy per initial state were used. For the angular distributions, 50000 trajectories were employed. Multisurface effects could be crudely included by multiplying the cross sections by 1/5, although the results here are presented without the multisurface factor.

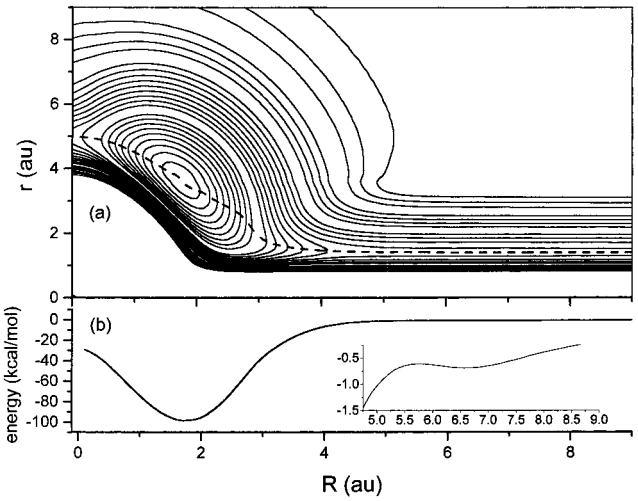

Figure 2. (a) Contour map of the H_2S PES as a function of R and r in the T-shape ($\theta = 90°$) geometry, where R and r are the Jacobi coordinates in the entrance channel. The dash line is the minimum-energy path. The contour energy increment is 6 kcal/mol from −100 to +90 kcal/mol, with the zero energy set to the two-atom limit $S(^1D) + H_2$. (b) Minimum-energy curve as a function of R. Inset in this plot is a blow-up portion for the range $R = 5.0-9.0\ a_0$. As is noticed, there is a small oscillation in this region.

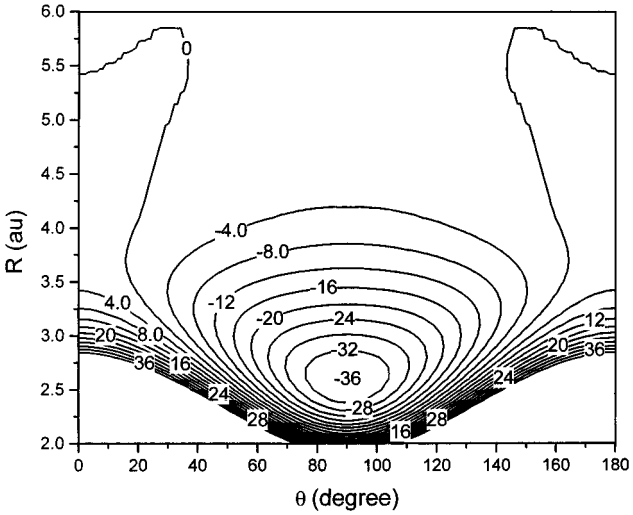

Figure 3. Contour map of the H_2S PES as a function of θ and R for $r = 1.4\ a_0$. The contour energy increment is 4 kcal/mol from −40 to 0 kcal/mol, with the zero energy set to the two-atom limit $S(^1D) + H_2$.

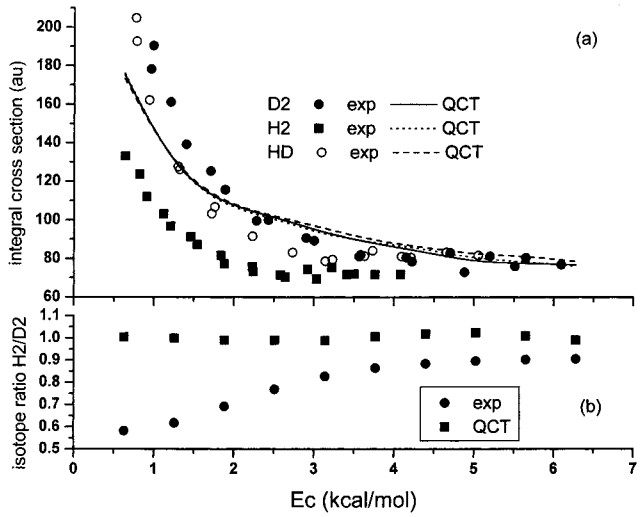

Figure 4. (a) Comparison of the experimental and the QCT excitation functions. The experimental data are normalized to the QCT data with respect to the highest energy D_2 data. The HD data is the sum of the two branches for the reaction S + HD → SD + H/SH + D. Notice that there is a mislabeling for the HD data in the experiment paper (see ref 45), so the correct isotope trend for the cross section is D_2 > HD > H_2 instead of HD > D_2 > H_2 in the original paper. (b) Energy dependence of the isotope ratio of H_2/D_2.

To perform a lifetime analysis on the complex-forming trajectories, we require a dynamical definition of the trapping time of a trajectory which separates out the asymptotic channel motion. Thus, we define the "lifetime", τ, to be

$$\tau = T_{\text{tot}} - R_{\text{initial}}/v_{\text{initial}} - R_{\text{final}}/v_{\text{final}} \qquad (5)$$

where T_{tot} is the total propagation time from the reactant channel to the product channel, R_{initial} and R_{final} are the initial and final values of the appropriate channel Jacobi distance, and v_{initial} and v_{final} are the asymptotic velocities. The last two terms in eq 5 correct for the free propagation of the trajectory. Of course eq 5 does not account for the influence of the centrifugal potential in the channels, but it is sufficiently accurate for our estimates.

III. Results

A. Integral Cross Sections and Isotope Effects. The QCT excitation functions, i.e., the dependence of the ICS on the translational collision energy E_C, for the reactions S(^{1}D) + H_2, S(^{1}D) + D_2, and S(^{1}D) + HD are presented in Figure 4a over the energy range 0.6−6 kcal/mol. The corresponding experimental data are also shown in the plot. We have normalized the experimental data with respect to the highest energy QCT result for the D_2 case (choosing another isotope would yield nearly identical results). The excitation functions all monotonically decrease with increasing collision energy. The QCT results are nearly the same for different isotopes, H_2, D_2, and HD. Such behavior is consistent with that predicted by the simple Langevin model of capture dynamics for a barrierless reaction. Although the corresponding experimental results show a similar falloff behavior, there are clear isotope effects, especially at the lower collision energies. The observed ordering is $\sigma(H_2) < \sigma(HD) < \sigma(D_2)$, where the H_2 results deviate most strongly from the other two.

If our scheme to normalize the experimental results at high energy is accepted, it is seen that the QCT results are in fairly good agreement with the data for D_2 and HD. It should be noted that the reported experimental errors are about 10% for the cross sections and about 5% in the collision energy calibration. Since the QCT results underestimate the excitation function by an amount of 5% for the lowest energy data, the result may be regarded as acceptable. On the other hand, the QCT result for the H_2 case is definitely in error since it overestimates the excitation function by 20% at low energy. Accompanying the excitation function, in Figure 4b we show the isotope ratio of H_2/D_2, which is independent of the normalization and thus more unambiguously shows the deviation between experiment and theory. Possible explanations for this isotope effect will be considered in the Discussion.

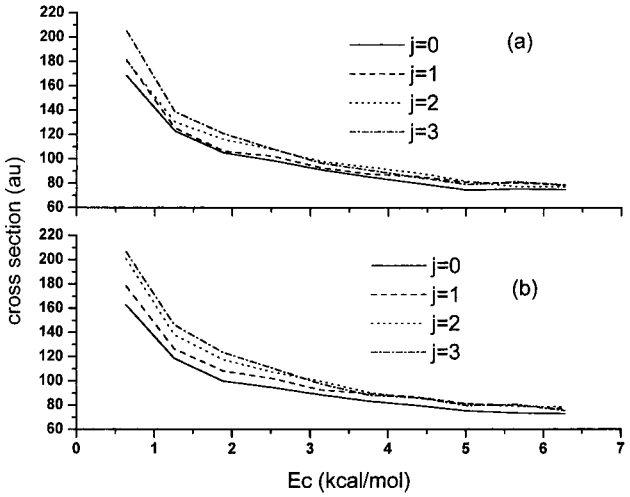

Figure 5. *j* dependence of the QCT excitation functions for the reactions (a) S + D_2 and (b) S + H_2.

It is also interesting to consider the effect of reagent rotation, *j*, on the excitation functions. In Figure 5, we see a modest yet significant *j* dependence for all the reactions. In general, it appears that the higher *j* states yield higher cross sections, with the largest effects on the order of 20%. A detailed analysis of the trajectory results indicates that the higher *j* states yield a larger capture radius, and thus a higher cross section. The decay probability into the product channel of a captured trajectory is nearly independent of *j*, consistent with statistical theory. We should point out that recent experimental results comparing para to ortho H_2 seems to indicate little or no *j* dependence.[61]

In Figure 6a, we show the excitation functions of the two product channels for the reaction S(^{1}D) + HD where the experiment is normalized with the same factor used in Figure 4. As can be seen in the plot, the QCT results are in better agreement with the data for the S(^{1}D) + HD → SH + D channel although there is significant underestimation of the integral cross sections in the lower energy region. On the other hand, there is a significant overestimation of the excitation function for the S(^{1}D) + HD → SD + H reaction, even in the high-energy region. Figure 6b shows that the QCT product branching ratio is reversed from the experimental result. That is, experiment shows σ(SH + D) > σ(SD + H) while the QCT gives the opposite ordering. The QCT result is again consistent with the statistical model of complex decay and previous bulk experimental results for other insertion reactions.[45] This is also the trend observed in the analogous O(^{1}D) reaction at low energies.[15,16] However, the experimental results show that the ratio is nearly constant (about 0.7) and is significantly lower than 1. This reversed isotope ratio suggests that there should be a bottleneck effect as the complex HSD decomposes to the product H + SD, as compared with the other branch.

B. Differential Cross Sections and Angle-Specific Energy Partitions. The differential cross sections (DCSs) at the two experimental energies for each reaction are displayed in Figure

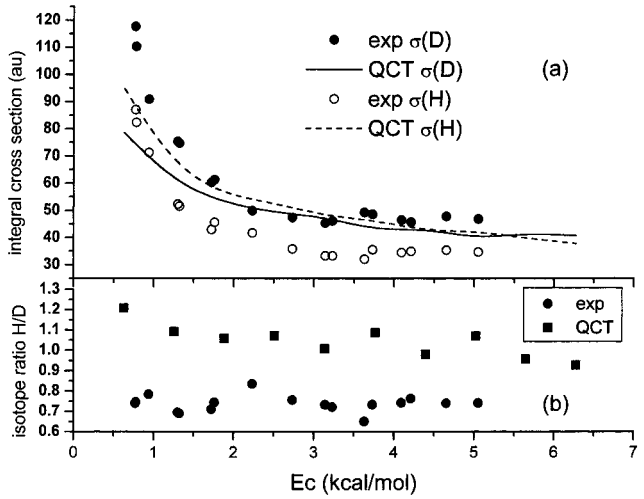

Figure 6. (a) Comparison of the experimental and the QCT excitation functions for the two product branches of the reaction S + HD. The normalization is the same as that described in Figure 4. σ(D) and σ(H) represent the two branches S + HD → SH + D and S + HD → SD + H, respectively. (b) Energy dependence of the isotope branching ratio of H/D.

7. [Note that the c.o.m. scattering angle, θ, is the relative angle between the outgoing vector of the H/D product and the incident vector of the diatomic molecule in the center-of-mass frame, which is $\pi-\theta$ using the conventional definition.[62]] The QCT and experiment show forward/backward peaking which is only weakly asymmetrical. This is quite similar to the distributions observed in the O(^{1}D) + H_2 system at low energy[22,23] and entirely consistent with the notion of the reaction proceeding through a long-lived complex. The experiment generally shows a higher contribution at the forward and backward directions than does the QCT. Furthermore, the change in the distribution with energy seems somewhat stronger in the experimental DCS. The (slight) asymmetry favoring forward over backward scattering is also qualitatively reproduced by the QCT.

We have computed the partitioning of excess product energy as a function of scattering angle. In Figure 8, the fraction of translational energy is in the lowest partition, the rotational energy is in the middle partition, and the vibrational energy (above the zero point) is in the highest partition. The QCT results, shown on the left, were gathered in 12 angular bins. The experimental results are shown on the right. It is seen that the magnitude of the energy partitioning is well reproduced by the QCT. Indeed, the angle-integrated partitioning presented in Table 1 indicates the QCT results are quantitatively accurate. The angular energy fractioning is nearly isotropic, as one might expect from a statistical decay theory. The experimental results show a small enhancement of the vibrational contribution for sideways scattering that is not reproduced by the QCT.

The angular distribution of j' states of HS and DS product molecules is shown in Figure 9. The scattering angle, j' quantum number, and v' quantum number are obtained using histogram binning with 50000 trajectories per energy. The forward/backward peaking of the distributions is somewhat masked by the implicit inclusion of the sin θ weighting factor, although it is still apparent for some of the $v' = 0$ results. The main feature of the distribution is the very high rotational excitation of the products. The QCT seems to reproduce the qualitative features of the observed product distribution, and the general magnitudes of the quantities, although the finer details of the distribution are of course different. Some traces of nonstatistical behavior are apparent in the angular structure of the product distribution.

C. Translational Energy Distribution. The translational energy distribution (TED), defined as $P(E_t) = d\sigma/dE_t$, provides more detailed information about the reaction dynamics than the averaged energy partitioning presented in the previous subsection. In Figure 10, we present the results for each reaction at the two experimental energies. The overall pattern of the TED is seen to be reasonably well reproduced by the QCT. The TED for the S(^{1}D) + D_2 reaction in particular is quite well modeled. On the other hand, the finer structure in the experimental TED is averaged out in the QCT. This is understandable since some of the "peaks" in the experimental results are likely the result of quantization of the final vibrational quantum number, which, of course, would not be modeled by classical mechanics. On the other hand, some of the structure in the TED is the result of bimodal distribution in the j' states, which in principle could be described classically.

The separate contribution from the product vibrational states can be modeled in the QCT by binning the final vibrational action of the product diatom. In Figures 11 and 12, the vibrationally resolved internal energy distribution ($E_{int} = E - E_t$) in the backward, sideways, and forward directions is compared to experiment for S(^{1}D) + D_2 and S(^{1}D) + H_2, respectively. The overall shapes of the distributions are roughly comparable. The magnitudes of the $v' = 1$ TED are generally far too low in the QCT, while that for $v' = 0$ is roughly correct. Table 2 shows the QCT and experimental vibration branching ratios for the reactions.

IV. Discussion

It is clear from the results that the reaction observables for S(^{1}D) + H_2, D_2, and HD are broadly consistent with the dynamics of insertion reactions. The QCT results are insertion type by construction since the single PES employed does not permit abstraction at the energies considered. The theoretical−experimental agreements on general features of the observables are encouraging for this general view of the reaction. In this section, we consider in somewhat more physical terms the character of the QCT dynamics, and also discuss the quite apparent differences with experiment.

The ICS results are dominantly determined by the dynamics of capture in the entrance channel. The falloff of the ICS with increasing E_C is characteristic of the decrease of the capture radius with increasing energy for systems with purely attractive potentials. The PES employed in this study has no barrier to insertion along the T-shaped geometry characterizing the minimum-energy path, but is strongly anisotropic with respect to the rotation angle of the diatom. The anisotropy modifies the effective capture radius and also leads to a dependence of the ICS on reagent rotation.

The overall reaction can be viewed as a sequence of two steps: first capture of the projectile to form a complex, and second decay of the complex forward into the reactive channel. Hence, the reaction probability for an ensemble of trajectories can be written as

$$P_R = P_c\kappa \tag{6}$$

where P_c is the capture probability and κ is the transmission coefficient to products. The ICS can be analogously written in terms of the capture cross section as

$$\sigma_R = \sigma_c\kappa \tag{7}$$

It is interesting to separately compute the energy dependence of the two factors to interpret the falloff of the ICS and to

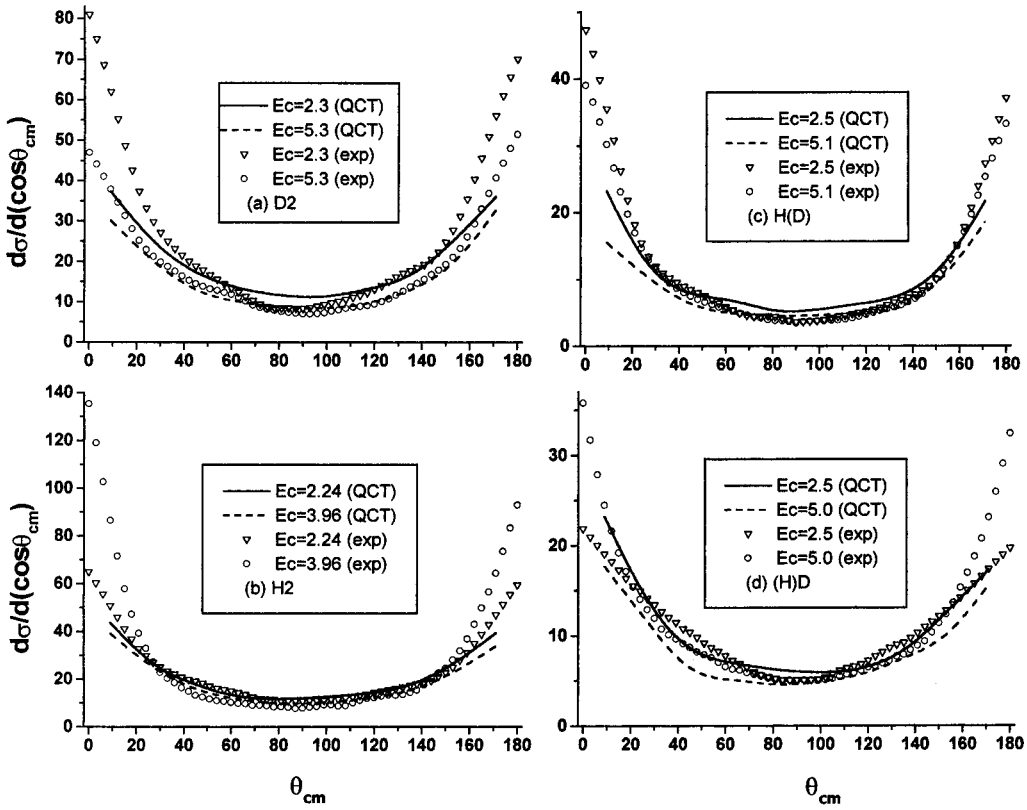

Figure 7. Differential cross sections for the reactions (a) S + D_2 → SD + D at E_c = 2.3 and 5.3 kcal/mol, (b) S + H_2 → SH + H at E_c = 2.24 and 3.96 kcal/mol, (c) S + HD → SH + D at E_c = 2.53 and 5.09 kcal/mol, and (d) S + HD → SD + H at E_c = 2.53 and 5.04 kcal/mol.

analyze the differences with experimental results. The capture probability of an ensemble requires a definition of a captured trajectory. From an inspection of the dynamics of many trajectories, we have noted that the H_2 bond distance r always distends further for a captured orbit. Thus, a captured trajectory is defined by $r > r_{min}$ at some point during its history, where r_{min} was set to 1.8 a_0 for $v = 0$. The product transmission probablity is defined formally from the reaction probability as

$$\kappa = P_R/P_c \tag{8}$$

In Figure 13, we see that σ_c shows the expected falloff with collision energy for all cases. The transmission probability, in contrast, is fairly flat with energy. The reagent rotation dependence is seen to be almost entirely due to the capture cross section, and reflects the anisotropy of the entrance channel potential.

The value of κ is somewhat smaller than expected from a pure statistical model of the captured trajectories.[63] A more detailed investigation of the captured trajectories reveals that a majority of the nonreactive-captured trajectories are quite short-lived, i.e., direct. Many of these trajectories show passage of the S atom almost directly through the center of mass of the diatom, which shows a large distension in bond length, and then direct exit of the S atom back into the reagent channel.[64] Since the inversion barrier on the PES for this process is about 24 kcal/mol below the reagent asymptote, such behavior occurs readily at low impact parameters. The remaining true complex trajectories decay into the entrance channel with a much lower probability, consistent with statistical phase space theory. We did not locate any significant number of direct-reactive trajectories.

The lifetime for decay of the complex can be obtained by fitting the long time survival probability of an ensemble of orbits to an exponential decay law. The complex lifetime will in general depend on both the total energy E and angular momentum J of the complex, and thus it is necessary to model the decay at each impact parameter in the QCT simulation. At fixed E, the lifetime increases with J since the centrifugal barriers to decay become higher. For example, as shown in Figure 14, the lifetime for S(^{1}D) + D_2 ($j = 0$) at E_c = 2.3 kcal/mol varies from 1.5 to 2.5 ps over the allowed range of impact parameters. (We should note that there is a small correction to the lifetimes computed by eq 5 due to the long-ranged centrifugal potential, which depends on b. We estimate the uncertainties introduced by this are 0.2 ps or less, which does not very significantly modify the results.) The lifetime at fixed J, on the other hand, monotonically decreases with increasing energy. For $J = 0$, the lifetime goes from 1.42 ps at 0.6 kcal/mol to 0.71 ps at 6 kcal/mol, as shown in Figure 15. The rotation constant for the H_2S molecule is about 9 cm^{-1}, so the rotation period of the complex is 0.33 ps at $J = 5$ and 0.17 ps at $J = 10$. Since the lifetime of the complex is significantly longer than the rotation period, the observed statistical distribution of the product distributions is to be expected.

Another way to view the capture dynamics is with the use of the opacity function, i.e., the reaction probability versus impact parameter, b, at fixed energy. The opacity functions are fairly flat out to the maximum impact parameter (at which point the centrifugal barrier height equals the translational energy) and then fall quickly to zero. The results for the S(^{1}D) + H_2 and S(^{1}D) + D_2 reactions are shown in parts a and b, respectively, of Figure 16. The slight increase in probability with increasing b reflects the decrease in the number of direct-nonreactive trajectories at higher impact parameter.

It is useful to consider the possible origin of differences between the experimental observations and the results of the QCT simulations. The list of possibilities is a rather long one.

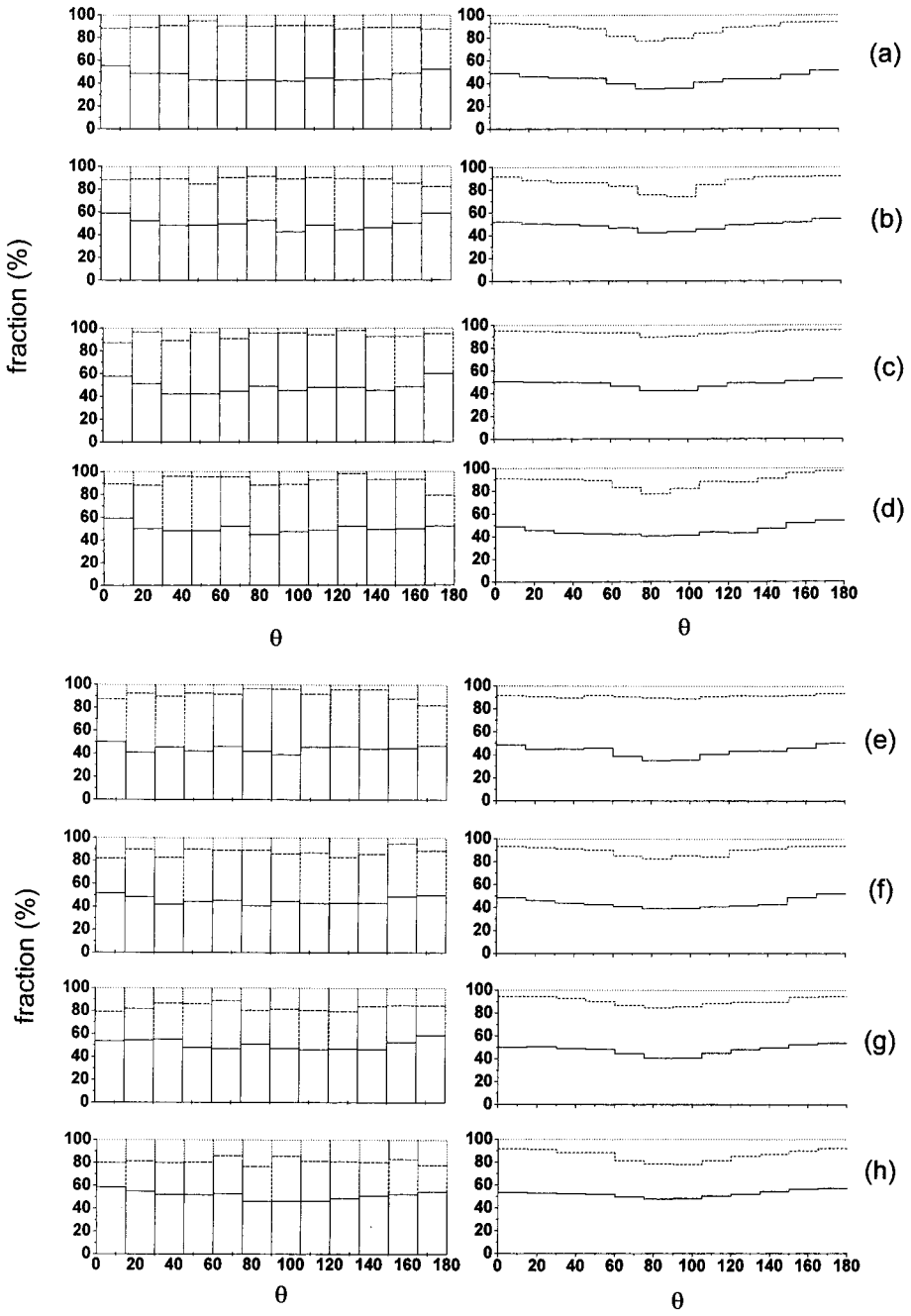

Figure 8. Angle-specific energy disposals: $S + D_2 \rightarrow SD + D$ at E_c = (a) 2.3 and (b) 5.3 kcal/mol, $S + H_2 \rightarrow SH + H$ at E_c = (c) 2.24 and (d) 3.96 kcal/mol, $S + HD \rightarrow SH + D$ at E_c = (e) 2.53 and (f) 5.09 kcal/mol, and $S + HD \rightarrow SD + H$ at E_c = (g) 2.53 and (h) 5.04 kcal/mol. The left panels are the QCT results, and the right ones are the experimental results. The disposals are represented by the relative fractions in percent.

TABLE 1: Comparison of the QCT (Numbers in the Parentheses) and the Experimental Results for the Fraction of the Averaged Kinetic and Internal Energy Release[a]

	E_c	$\langle f_T \rangle$	$\langle f_R \rangle$	$\langle f_V \rangle$
$S + D_2 \rightarrow SD + D$	2.3	43.4 (46.1)	44.6 (43.5)	12.0 (10.4)
	5.3	48.6 (49.8)	37.6 (37.0)	13.8 (13.2)
$S + H_2 \rightarrow SH + H$	2.24	48.0 (47.8)	45.3 (45.1)	6.7 (7.1)
	3.96	45.4 (49.7)	43.6 (41.2)	11.0 (9.1)
$S + HD \rightarrow SH + D$	2.53	43.3 (44.5)	47.6 (47.1)	9.1 (8.4)
	5.09	44.0 (44.8)	45.7 (42.4)	10.3 (12.8)
$S + HD \rightarrow SD + H$	2.53	47.4 (50.2)	42.6 (33.0)	10.0 (16.8)
	5.04	52.1 (51.1)	33.7 (29.6)	14.2 (19.3)

[a] The collision energy E_c is in kilocalories per mole. $\langle f_T \rangle$, $\langle f_R \rangle$, and $\langle f_V \rangle$ represent the fraction (%) for translation, rotation, and vibration motions, respectively.

Obviously, we need to worry about the accuracy of the PES. Most serious for the ICS results are errors in the entrance channel. Indeed, we noted previously that a higher level calculation at a small number of entrance channel geometries reveals that the true potential may be somewhat more attractive than our PES.[53] This is at least partially responsible for the more rapid falloff in the ICS seen in the experiment. Inaccuracies in the well and exit channel regions will lead to errors in the DCS and product distributions. It is clear that the surface is insufficiently accurate to reproduce at least the finer features of the state-resolved angular product distributions.

Similar to the analogous $O(^1D) + H_2$ reaction, it is very likely that nonadiabatic effects can play some role in the reaction as well. Although the energetic barrier to abstraction is fairly high, it is still certainly conceivable that nonadiabatic coupling to the 2A′ surface may contribute due to short-range electrostatic interaction via conical intersection. It is also possible that the

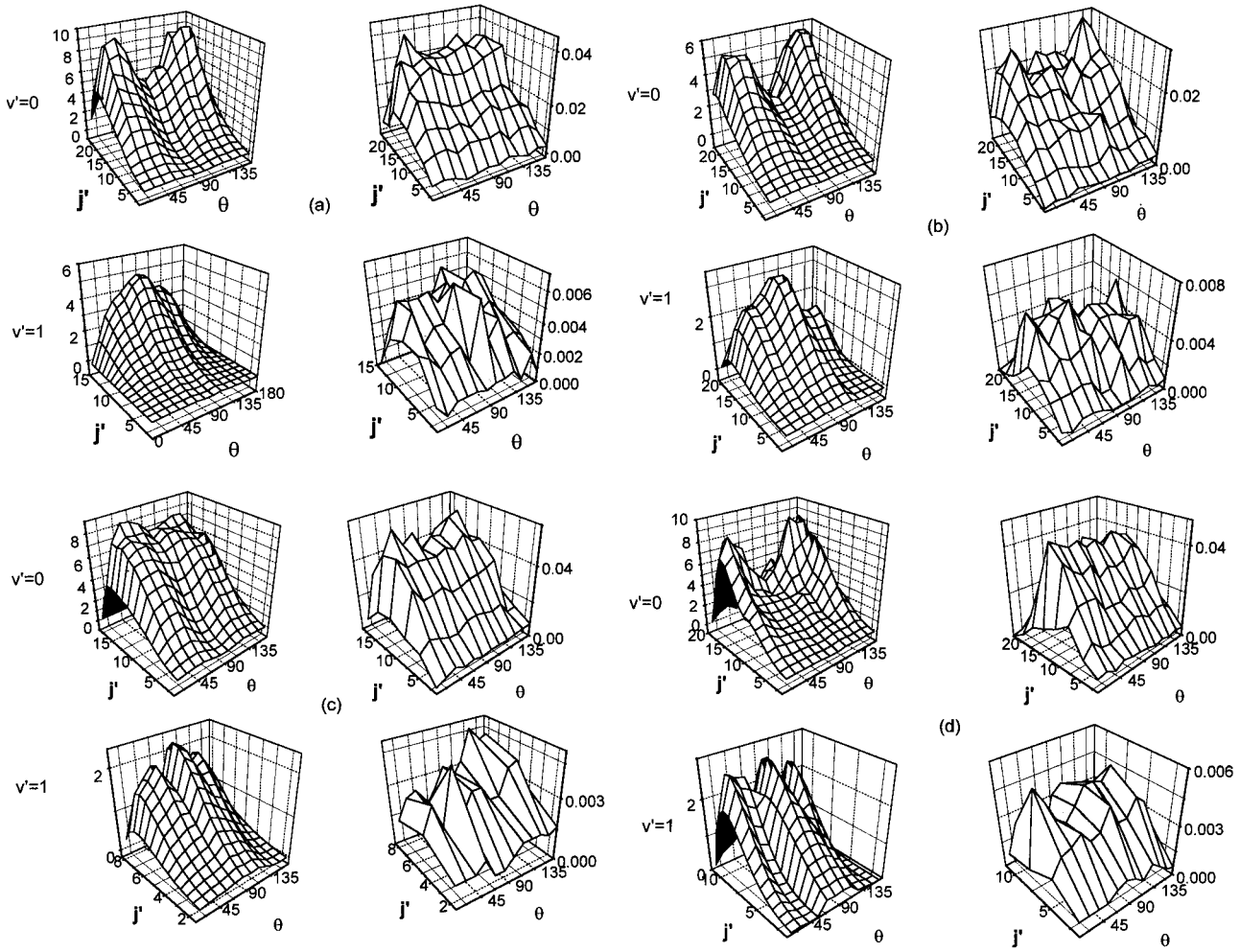

Figure 9. Rovibational state-specific angular product distributions for the reactions S + D_2 → SD + D at E_c = (a) 2.3 and (b) 5.3 kcal/mol and S + H_2 → SH + H at E_c = (c) 2.24 and (d) 3.96 kcal/mol. The experimental results are shown in the left panel and the QCT results shown in the right.

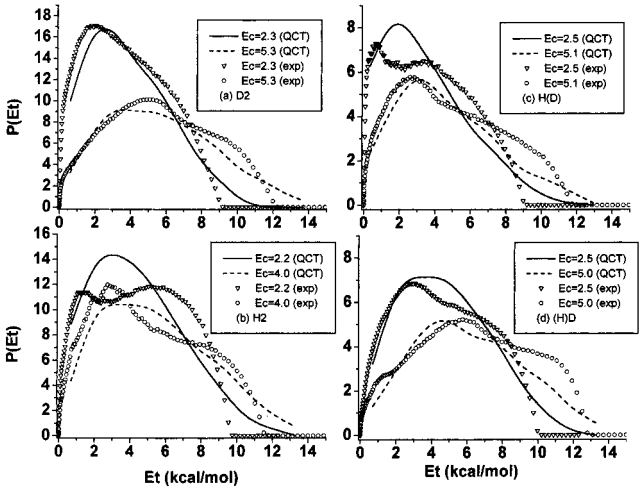

Figure 10. Product translation energy (E_t) distribution for the reactions (a) S + D_2 → SD + D at E_c = 2.3 and 5.3 kcal/mol, (b) S + H_2 → SH + H at E_c = 2.24 and 3.96 kcal/mol, (c) S + HD → SH + D at E_c = 2.53 and 5.09 kcal/mol, and (d) S + HD → SD + H at E_c = 2.53 and 5.04 kcal/mol.

reaction on the 1A″ surface may occur through long-range electrostatic interaction and/or Coriolis interaction, even though there is no significant nonadiabatic coupling to the 1A′ and 2A′ surfaces. As a matter of fact, for reactions involving open-shell atoms, it is not uncommon to find the two A′ states split from the Σ and Π surfaces interact through conical intersection, while the A′ and A″ states interact through Renner−Teller coupling, aside from the other possible nonadiabatic effects such as spin−orbit interactions.

We also should consider the possible role of quantum effects in the nuclear dynamics that are not included in the QCT simulations. We need to distinguish quantum mechanical corrections to the capture dynamics from that of the complex decay. Possible entrance channel quantum effects influencing capture include tunneling and reflection associated with the centrifugal barrier, and internal quantum effects of the rotation/vibration of the target diatom. Using semiclassical theory, we have estimated the tunneling and above the barrier reflection from the centrifugal barriers which contribute to the reaction. The net effects are quite small, 5% or less, and probably not important here. The quantum effects associated with the internal states of the diatom may play a larger role. If the dynamics in the entrance channel are assumed to be adiabatic, in the sense that the vibrational and rotational/bending quantum numbers are conserved along the reaction coordinate, there can be a large correction to the height of the dynamical barrier to reaction due to changes in the rovibrational frequencies. Because of its high frequency, the vibrationally adiabatic correction to the reaction barrier is probably reasonably reproduced by the QCT since the initially quantized vibrational action is accurately conserved classically. However, the low-frequency rotation/bending correction may show a much stronger quantum correction since

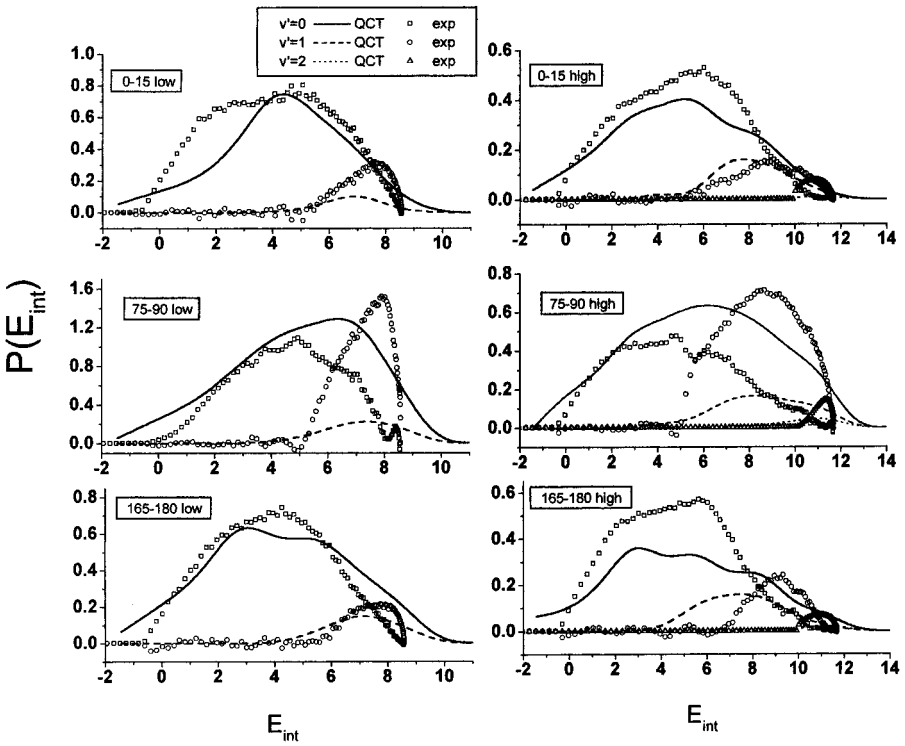

Figure 11. Partition of the angle-specific internal energy distributions for S + D_2 into the SD vibrational-state manifolds. Only three different angle segments (0−15°, 75−90°, and 165−180°) are shown here to display the crucial difference. The low energy refers to E_c = 2.3 kcal/mol and the higher one to E_c = 5.3 kcal/mol.

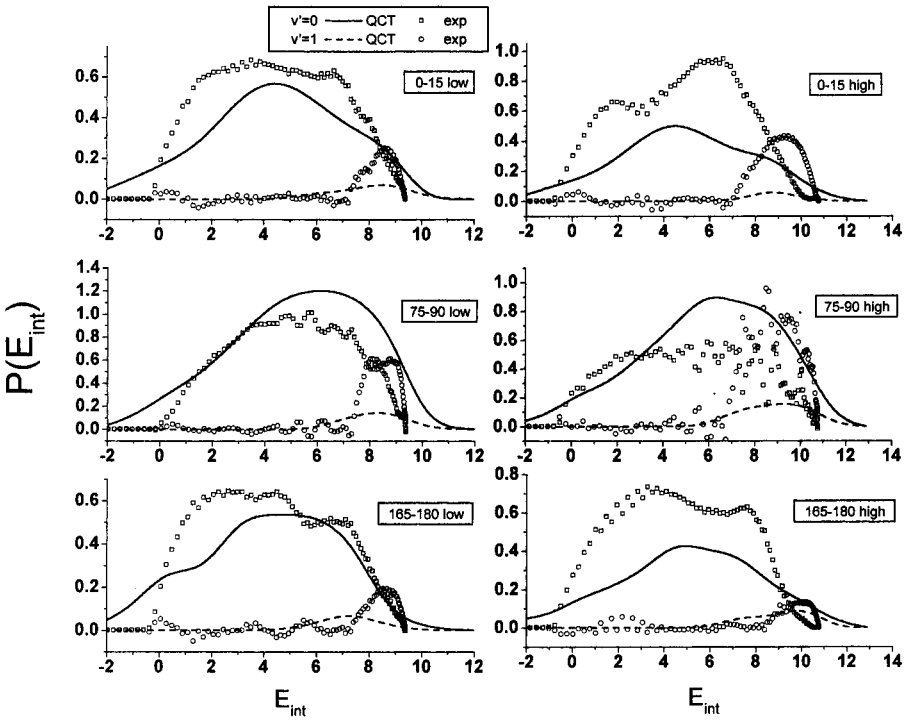

Figure 12. Same as Figure 11, but for the reaction S + H_2 → SH + H. The low energy refers to E_c = 2.24 kcal/mol and the higher one to E_c = 3.96 kcal/mol.

classical adiabaticity for this mode is violated. This could cause a significant isotope effect since the adiabatic contribution to the dynamical barrier height depends strongly on the mass and quantum number. Indeed, it is conceivable that the isotope effect observed in the experimental ICS is the byproduct of the higher adiabatic barrier expected for the lighter atoms, which should therefore suppress the ICS for the H_2 case in particular.

We expect quantum effects in the complex decay should include, as a major contribution, the role of quantization of vibrational states in the exit channels. Since the vibrational zero-point energy is higher in the entrance channel than in the exit channel, we expect quantum mechanics will increase the forward decay probability into products compared with the QCT. However, on the basis of an RRKM analysis,[63] there does not appear to be a significant change in the branching ratio of decay products versus energy in the energy regime we have treated.

TABLE 2: Comparison of the QCT (Numbers in Parentheses) and the Experimental Results for the Vibrational Branching Ratios[a]

	E_c	$\langle P_0 \rangle$	$\langle P_1 \rangle$	$\langle P_2 \rangle$
$S + D_2 \rightarrow SD + D$	2.3	0.80 (0.91)	0.20 (0.09)	
	5.3	0.72 (0.85)	0.26 (0.14)	0.02 (0.01)
$S + H_2 \rightarrow SH + H$	2.24	0.92 (0.96)	0.08 (0.04)	
	3.96	0.84 (0.93)	0.16 (0.07)	
$S + HD \rightarrow SH + D$	2.53	0.90 (0.95)	0.10 (0.05)	
	5.09	0.85 (0.90)	0.15 (0.10)	
$S + HD \rightarrow SD + H$	2.53	0.82 (0.86)	0.18 (0.14)	
	5.04	0.71 (0.80)	0.25 (0.18)	0.04 (0.02)

[a] The collision energy E_c is in kilocalories per mole. $\langle P_0 \rangle$, $\langle P_1 \rangle$, and $\langle P_2 \rangle$ represent the ratios for the $v' = 0$, $v' = 1$, and $v' = 2$ states, respectively.

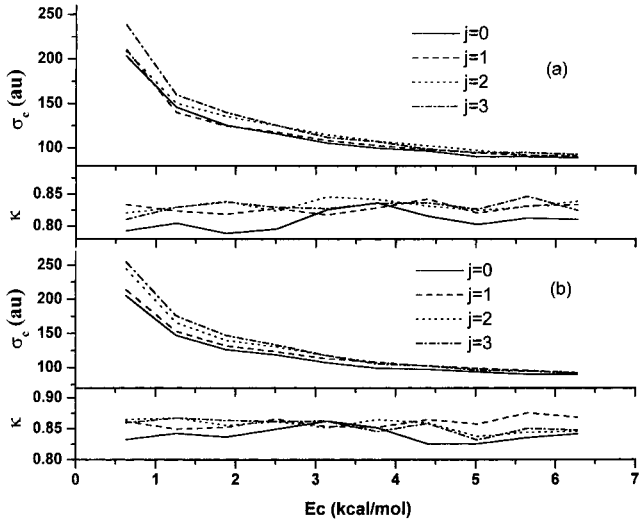

Figure 13. Energy dependence of σ_c and κ for the reactions (a) $S + D_2$ and (b) $S + H_2$.

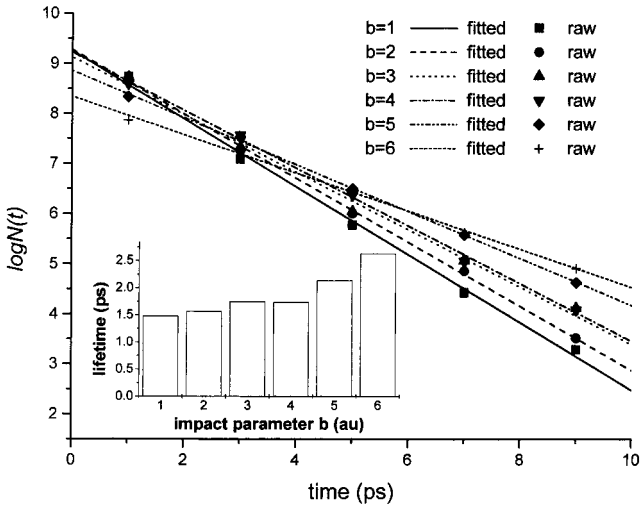

Figure 14. Decay curves for the $S + D_2$ ($j = 0$) reaction at $E_c = 2.3$ kcal/mol. Inset in the plot is the b dependence of the fitted lifetimes.

Indeed, the quantum transmission probability remains close to 1 over the whole energy range. Thus, it appears unlikely that such quantum effects will change the shape of the ICS curve. We should also consider the influence of vibrational quantization in the exit channels on the product branching ratio for the $S(^1D) + HD$ reaction. As seen in Figure 6, the QCT results favor the $DS + H$ channel at low energy, with the branching ratio going to 1 at high energy; on the other hand, the experiment shows a different result, with the $HS + D$ channel preferred at all

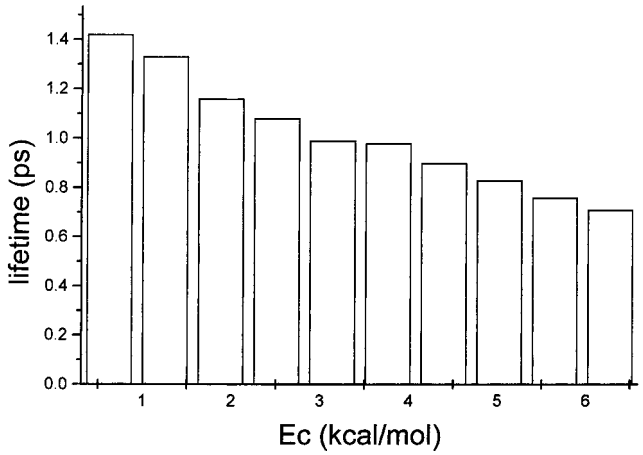

Figure 15. Energy dependence of the fitted lifetimes for the $S + D_2$ ($j = 0$) reaction at $J = 0$.

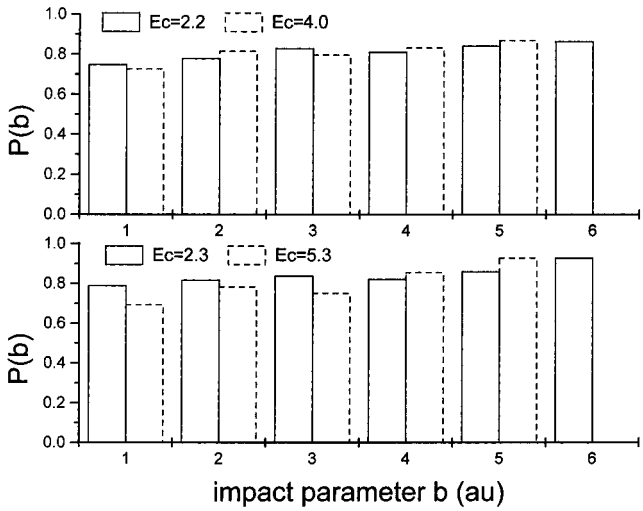

Figure 16. Opacity functions for the reactions $S + H_2$ (a, upper panel) and $S + D_2$ (b, lower panel) at their corresponding experimental collision energies in kilocalories per mole.

energies. If the zero-point energy constraint is applied to the exit channels, we expect the effective barrier to decay into the $HS + D$ channel to be raised by a larger amount than that for $DS + H$. Thus, it would seem that imposing the quantization constraint would push the QCT results into worse disagreement with experiment.

In summary, the QCT results are for the most part consistent with the simple capture-statistical decay picture of insertion dynamics. This simple picture can account, at least qualitatively, for many aspects of the experimental observations such as the ICS, the state-averaged DCS, and the angle-averaged product distributions. Nonstatistical effects observed in the experimental measurements, such as in the angle-state-resolved product distribution and a product branching ratio, apparently involve dynamical phenomena which go beyond our model. More ambitious calculations involving multiple PESs will likely be required to bring the results of theory in line with experiment.

Acknowledgment. We thank K. Liu and S.-H. Lee for useful discussions of their experimental findings. We are grateful to H. Rabitz and T. Hollebeek for providing the RKHS fitting code. We have also benefited from discussions with A. Zyubin and A. Mebel concerning the PES. This work is financially supported by the National Science Foundation.

References and Notes

(1) Kobayashi, H.; Takayanagi, T.; Tsunashima, S. *Chem. Phys. Lett.* **1997**, *277*, 20.
(2) Pederson, L. A.; George, G. C.; Ho, T.-S.; Hollebeek, T.; Rabitz, H.; Harding, L. B.; Lendvay, G. *J. Chem. Phys.* **1999**, *110*, 9091.
(3) Casavecchia, P.; Balucani, N.; Alagia, M.; Cartechini, L.; Volpi, G. G. *Acc. Chem. Res.* **1999**, *32*, 503.
(4) Honvault, P.; Launay, J.-M. *J. Chem. Phys.* **1999**, *111*, 6665.
(5) Umemoto, H.; Terada, N.; Tanaka, K. *J. Chem. Phys.* **2000**, *112*, 5762.
(6) Rudich, Y.; Hurwitz, Y.; Frost, G. J.; Vaida, V.; Naaman, R. *J. Chem. Phys.* **1993**, *99*, 4500.
(7) Arai, H.; Kato, S.; Koda, S. *J. Phys. Chem.* **1994**, *98*, 12.
(8) van Zee, R. D.; Stephenson, J. C. *J. Chem. Phys.* **1995**, *102*, 6946.
(9) Hack, W.; Thiesemann, T. *J. Phys. Chem.* **1995**, *99*, 17364.
(10) Lin, J. J.; Lee, Y. T.; Yang, X. *J. Chem. Phys.* **1998**, *109*, 2975.
(11) Buss, R. J.; Casavecchia, P.; Hirooka, T.; Sibener, S. J.; Lee, Y. T. *Chem. Phys. Lett.* **1981**, *82*, 386.
(12) Laurent, T.; Naik, P. D.; Volpp, H. R.; Wolfrum, J.; Arusi-Parpar, T.; Bar, I.; Rosenwaks, S. *Chem. Phys. Lett.* **1995**, *236*, 343.
(13) Che, D.-C.; Liu, K. *J. Chem. Phys.* **1995**, *103*, 5164.
(14) Alexander, A. J.; Aoiz, F. J.; Brouard, M.; Burak, I.; Fujimura, Y.; Short, J.; Simons, J. P. *Chem. Phys. Lett.* **1996**, *262*, 589.
(15) Hsu, Y.-T.; Liu, K. *J. Chem. Phys.* **1997**, *107*, 1664.
(16) Hsu, Y.-T.; Wang, J. H.; Liu, K. *J. Chem. Phys.* **1997**, *107*, 2351.
(17) Alexander, A. J.; Blunt, D. A.; Brouard, M.; Simons, J. P.; Aoiz, F. J.; Banares, L.; Fujimura, Y.; Tsubouchi, M. *Faraday Discuss.* **1997**, *108*, 375.
(18) Alagia, M.; Balucani, N.; Cartechini, L.; Casavecchia, P.; van Kleef, E. H.; Volpi, G. C.; Kuntz, P. J.; Sloan, J. J. *J. Chem. Phys.* **1998**, *108*, 6698.
(19) Ahmed, M.; Peterka, D. S.; Suits, A. G. *Chem. Phys. Lett.* **1999**, *301*, 372.
(20) Lee, S.-H.; Liu, K. *J. Chem. Phys.* **1999**, *111*, 4351.
(21) Hsu, Y.-T.; Liu, K.; Pederson, L. A.; Schatz, G. C. *J. Chem. Phys.* **1999**, *111*, 7921, 7931.
(22) Hermine, P.; Hsu, Y.-T.; Liu, K. *Phys. Chem. Chem. Phys.* **2000**, *2*, 581.
(23) Liu, X.; Lin, J. J.; Harich, S. A.; Yang, X. *J. Chem. Phys.* **2000**, *113*, 1325.
(24) Sorbie, K. S.; Murrell, J. N. *Mol. Phys.* **1975**, *29*, 1387.
(25) Schinke, R.; and Lester, W. A., Jr. *J. Chem. Phys.* **1980**, *72*, 3754.
(26) Murrell, J. N.; Carter, S. *J. Phys. Chem.* **1984**, *88*, 4887.
(27) Murrell, J. N.; Carter, S.; Farantos, S. C.; Huxley, P.; Varandas, A. J. C. *Molecular Potential Functions*; Wiley: Chichester, 1984.
(28) Ho, T.-S.; Hollebeek, T.; Rabitz, H.; Harding, L. B.; Schatz, G. C. *J. Chem. Phys.* **1996**, *105*, 10472.
(29) Dobbyn, A. J.; Knowles, P. J. *Mol. Phys.* **1997**, *91*, 1107.
(30) Fitzcharles, M. S.; Schatz, G. C. *J. Phys. Chem.* **1986**, *90*, 3634.
(31) Walch, S. P.; Harding, L. B. *J. Chem. Phys.* **1988**, *88*, 7653.
(32) Goldfield, E. M.; Wiesenfeld, J. R. *J. Chem. Phys.* **1990**, *93*, 1030.
(33) Schatz, G. C.; Papaioannou, A.; Peterson, L. A.; Harding, L. B.; Ho, T.-S.; Hollebeek, T.; Rabitz, H. *J. Chem. Phys.* **1997**, *107*, 2340.
(34) Alexander, A. J.; Aoiz, F. J.; Banares, L.; Brouard, M.; Simons, J. P. *Phys. Chem. Chem. Phys.* **2000**, *2*, 571.
(35) Whitlock, P. A.; Muckerman, J. T.; Fisher, E. R. *J. Chem. Phys.* **1982**, *76*, 4468.
(36) , Kuntz, P. J.; Niefer, B. I.; Sloan, J. J. *J. Chem. Phys.* **1988**, *88*, 3629.
(37) Kuntz, P. J.; Niefer, B. I.; Sloan, J. J. *Chem. Phys.* **1991**, *151*, 77.
(38) Schatz, G. C.; Pederson, L. A.; Kuntz, P. J. *Faraday Discuss.* **1997**, *108*, 357.
(39) Badenhoop, J. K.; Koizumi, H.; Schatz, G. C. *J. Chem. Phys.* **1989**, *91*, 142.
(40) Peng, T.; Zhang, D. H.; Zhang, J. Z. H.; Schinke, R. *Chem. Phys. Lett.* **1996**, *248*, 37.
(41) Dai, J. *J. Chem. Phys.* **1997**, *107*, 4934.
(42) Balint-Kurti, G. G.; Gonzalez, A. I.; Goldfield, E. M.; Gray, S. K. *Faraday Discuss.* **1998**, *110*, 169.
(43) , Gray, S. K.; Goldfield, E. M.; Schatz, G. C.; Balint-Kurtii, G. G. *Phys. Chem. Chem. Phys.* **1999**, *1*, 1141.
(44) Drukker, K.; Schatz, G. C. *J. Chem. Phys.* **1999**, *111*, 2451.
(45) Lee, S.-H.; Liu, K. *Chem. Phys. Lett.* **1998**, *290*, 323; erratum **2000**, *317*, 516.
(46) Lee, S.-H.; Liu, K. *J. Phys. Chem.* **1998**, *102*, 8637.
(47) Lee, S.-H.; Liu, K. In *Advances in Molecular Bean Research and Applications*; Campargue, R., Ed.; Springer-Verlag: Berlin, 2000.
(48) Lee, S.-H.; Liu, K. Unpublished data.
(49) Heumann, B.; Welde, K.; Duren, R.; Schinke, R. *J. Chem. Phys.* **1993**, *98*, 5508.
(50) Stevens, J. E.; Chaudhuri, R. K.; Freed, K. F. *J. Chem. Phys.* **1996**, *105*, 8754.
(51) Pericou-Cayere, M.; Gelize, M.; Dargelos, A. *Chem. Phys.* **1997**, *214*, 81.
(52) Simah, D.; Hartke, B.; Werner, H.-J. *J. Chem. Phys.* **1999**, *111*, 4523.
(53) Zyubin, A. S.; Mebel, A. M.; Chao, S. D.; Skodje, R. T. *J. Chem. Phys.*, in press.
(54) Woon, D. E.; Dunning, T. H., Jr. *J. Chem. Phys.* **1993**, *98*, 1358.
(55) Dunning, T. H., Jr. *J. Chem. Phys.* **1989**, *90*, 1007.
(56) Silver, D. W.; Davidson, E. R. *Chem. Phys. Lett.* **1978**, *52*, 403.
(57) Ho, T.-S.; Rabitz, H. *J. Chem. Phys.* **1996**, *104*, 2584 and references therein.
(58) Bunker, D. L. *Methods Comput. Phys.* **1971**, *10*, 287.
(59) Porter, R. N.; Raff, L. M. In *Dynamics of Molecular Collision*; Miller, W. H., Ed.; Plenum: New York, 1976.
(60) Truhlar, D. G.; Muckerman, J. T. In *Atom-molecule Collision Theory*; Bernstein, R. B., Ed.; Plenum: New York, 1979.
(61) Liu, K. Private communication.
(62) Levine, R. D.; Bernstein, R. B. *Molecular reaction dynamics and chemical reactivity*; Oxford University: Oxford, 1987.
(63) Chang, A. H. H.; Lin, S. H. *Chem. Phys. Lett.* **2000**, *320*, 161.
(64) Guadagnini, R.; Schatz, G. C. *J. Phys. Chem.* **1996**, *100*, 18944.